JOURNAL OF GEOPHYSICAL RESEARCH, VOL. 106, NO. C10, PAGES 22,313–22,329, OCTOBER 15, 2001

General circulation and intergyre dynamics in the eastern North Atlantic from a regional primitive equation model

Thierry Penduff[1]

Laboratoire des Ecoulements Géophysiques et Industriels, Grenoble, France

Alain Colin de Verdière

Laboratoire de Physique des Océans, Université de Bretagne Occidentale, Brest, France

Bernard Barnier

Laboratoire des Ecoulements Géophysiques et Industriels, Grenoble, France

Abstract. The mean circulation of the eastern North Atlantic is investigated using a regional 0.8°× cos(latitude)-resolution configuration of the SPEM primitive equation sigma coordinate model, forced by seasonal and monthly surface fluxes. The computational domain is surrounded by three self-adapting open boundaries which evacuate the outgoing perturbations and laterally control the baroclinic modes in inflow regions, but let the model adjust the barotropic mode to a large extent. The final solution is stable and reproduces most features of the basin's mean circulation well: A realistic Azores Current, the observed paths and transports of subpolar currents, of the branches of the North Atlantic Current, of the intergyre zone modal and intermediate water masses down to about 2000 m. Some unrealistic circulation features, attributed to the modest resolution and to certain limitations of the sigma coordinates, are found below 2000 m. The buoyancy and vorticity balances are investigated in the intergyre zone. The Subpolar Mode Water (SPMW), subducted at a realistic rate, continues its southward journey toward the ocean's interior in accordance with the ventilated thermocline theory, with eddy diapycnal fluxes exerting a moderating effect. The poleward motion observed between 300 and 1000 m is well reproduced north of 45°N and governed by similar dynamics, but is absent south of 45°N within the upper Mediterranean Water.

1. Introduction

The mean circulation and dynamics of the North Atlantic Ocean are better known west of the Mid-Atlantic Ridge (MAR) than east of it. This situation has historical origins but still persists, probably because the ocean dynamics differ between the two basins. In the western basin the mean flow is dominated by the Gulf Stream extension, a permanent, intense and thin (about 100 km-wide) jet that remains confined within a rather limited area (about 2°-wide [*Kelly,* 1991]). East of 45°W the major current (North Atlantic Current, NAC) is weaker and splits into several branches whose number, intensity, *T-S* structure, and path are subject to intense interannual variability [*Sy et al.,* 1992]. Other major features of the mean circulation in the eastern basin, such as the warm water export toward the Norwegian Sea [*Orvik et al.,* 1999], its return flow above the Greenland-Iceland-Scotland sills [*Bacon,* 1998], or the current regime between the subpolar and the subtropical gyres [*Sy,* 1988] are linked with the NAC and also exhibit an important interannual variability.

Present estimates of the large-scale circulation in the basin are thus restricted to given periods, areas or immersions: The early eighties [*Sy,* 1988; *Arhan et al.,* 1989; *Sy et al.,* 1992; *Gana and Provost,* 1993], the late winter in the eighties [*Paillet and Mercier,* 1997] (noted PM97 thereafter), the near-surface mean circulation during the eighties [*Brügge,* 1995], or the early nineties [*Otto and van Aken,* 1996]. *Schmitz and McCartney* [1993, p. 29] proposed a synthesis of numerous local measurements and schemes of the North Atlantic mean circulation, but pointed out that "there are still significant gaps in our knowledge of [this] circulation."

Among available in situ measurements, hydrographic data are the most abundant east of the MAR and constitute an interesting starting point to evaluate the mean circulation. However, hydrography-based direct estimates of transports across individual sections may not

[1]Now at Center for Ocean-Atmospheric Prediction Studies, Florida State University, Tallahassee, Florida, USA.

Paper number 2000JC000346.
0148-0227/01/2000JC000346$09.00

accurately represent the dynamical impact of topography on the large-scale flow, shown to be crucial at these latitudes [*Wunsch and Roemmich*, 1985; *Arhan et al.*, 1989], because a level of no motion has to be chosen. This choice is partly arbitrary, has a significant impact on the total transport [PM97], and certainly distorts the topographic effect. In addition to the interannual variability, this explains why geostrophic estimates of the NAC transport above the MAR cover a wide range [see *Sy et al.*, 1992, Table 2]. North of about 40°N, geostrophic estimates of the current transports should thus be interpreted with caution.

One may also deduce the mean flow in the basin from a set of dynamical equations and a T-S annual climatology based on several decades of hydrographic data. A mean velocity field representative of these decades may be computed from such a stratification by an inverse model (as was done for one particular season by PM97), but the possible mean contribution of the wind- and buoyancy-driven variability cannot be addressed. Our approach is to initialize a prognostic non-eddy-resolving primitive equation model of the basin with a climatological T-S stratification representative of a given season, and to integrate the model with a realistic seasonal forcing until stabilization. The final mean stratification and circulation are thus adjusted mutually and to the surface and lateral forcing, and explicitly integrate the ocean variability up to seasonal timescales. Provided that the model, its lateral and surface forcings are reliable, and that the spin-up leads to a realistic and stable solution, this prognostic approach helps to complement in situ or inverse estimates of the mean circulation. This is the first aim of the present study.

Our second goal is to investigate the origin of subsurface currents in the so-called intergyre region, located between the NAC and the Azores Current (AC). The ventilated thermocline theory [*Luyten et al*, 1983] provides an explanation of the way in which layers lying below a directly wind-driven surface layer can be put into motion: In regions of downward Ekman pumping, fluid columns can be subducted beneath the surface layer and continue their southward journey conserving their low potential vorticity acquired at outcrop lines. An important result of this adiabatic calculation was the appearance of shadow zones along eastern boundaries, which occur due to the strict adherence to the conditions of potential vorticity conservation and zero normal geostrophic velocity at the eastern boundary. An-

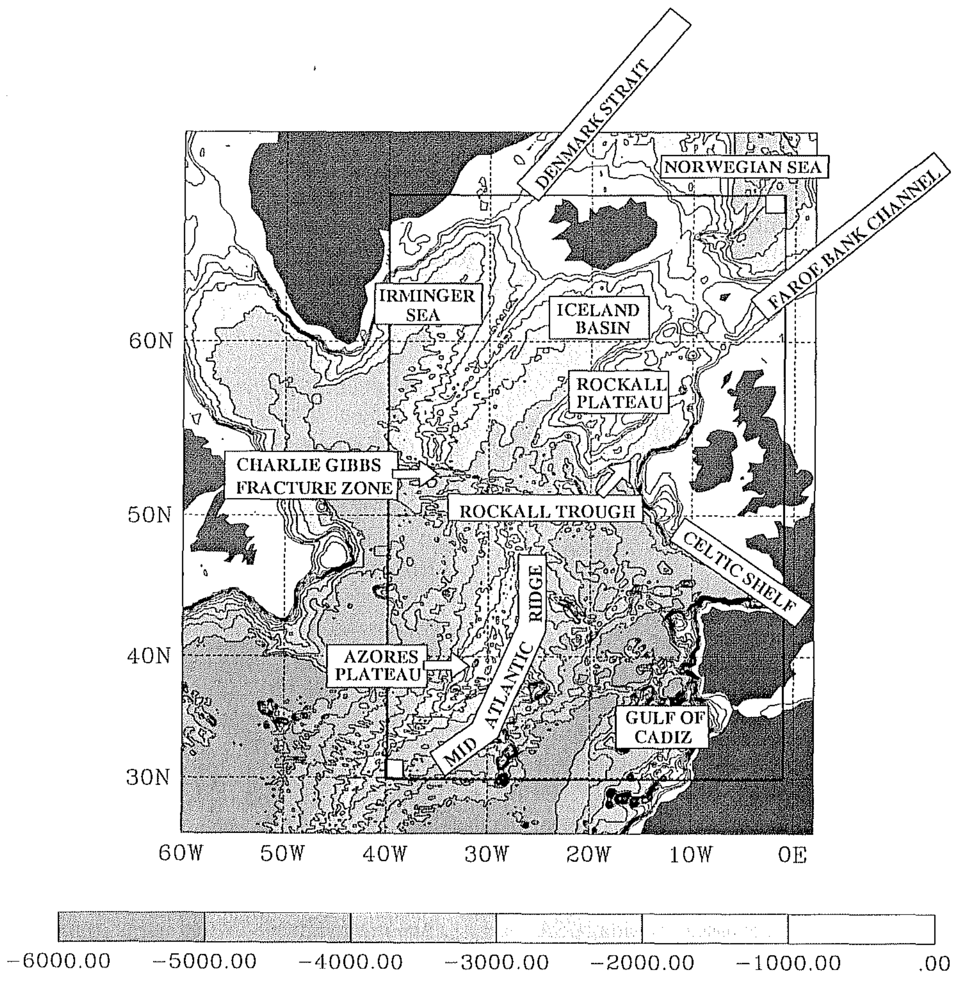

Figure 1. The eastern North Atlantic original topography. Straight lines represent the computational domain limits.

other way of putting deep layers in motion is through internal turbulent diffusion. *Luyten and Stommel* [1986] describe case studies in which solutions appropriate to the subtropical gyre heating, subpolar gyre cooling, and wind stress distributions are obtained through Sverdrup dynamics. Although the surface stress distribution can be considered as given, it is another matter for the heating-cooling distributions that are closely interrelated with the large-scale advection field one wishes to calculate. An alternative to the arbitrary distribution of their cross-isopycnal flux is to "observe" the links between the large-scale circulation and the turbulent forcing fields in a numerical model, and to interpret those links at the level of Sverdrup dynamics. For this to be a fruitful exercise, the model solution should be close to the real circulation so that the motions of known water masses can be associated with different contributions to the stretching term in the planetary vorticity equation. Once our eastern North Atlantic model produces realistic flow rates for the water masses, we shall investigate how the Subpolar Mode Water and the Mediterranean Water are set in motion.

To date, the results of several North Atlantic models have been published and a number of comparisons made [*Tréguier,* 1992; *Bryan et al.,* 1995; *DYNAMO Group,* 1997]. These comparisons reveal significant differences and discrepancies east of the MAR (distorted and weak NAC, absence of the AC), even at high resolution. These weaknesses may be linked to the inability of most basin-scale models to reproduce the Gulf Stream separation process properly. Our numerical domain was thus restricted to the eastern basin through the use of "self-adapting" open boundaries [*Penduff et al.,* 2000] (noted P00 hereafter), partly controlled by recent climatological *T-S* fields.

The paper is divided into several sections. In section 2 we briefly summarize the model configuration. In section 3 the final mean circulation is described and compared with available estimates. The impact of internal diffusive processes on the motion of the water masses in the intergyre zone is investigated in section 4. Our results are summarized in section 5.

2. Model Configuration

The present study is conducted using the SPEM5.1 primitive equation model at a resolution of 0.8° in longitude and 0.8°× cos(ϕ) in latitude ϕ. The limits of the study area are justified in P00 and shown in Figure 1. SPEM uses sigma coordinates on the vertical, which allow a more natural treatment of the bottom topography condition. The possible tendency of geopotential coordinate models to overestimate the blocking effect of the MAR [*Tréguier,* 1992] is also avoided with this approach. In order to limit the spurious velocities generated by truncation errors in the pressure gradient calculation, the topography was smoothed using the criterion adopted by *Barnier et al.* [1998] and validated in a "resting stratification case" (see the latter paper). The actual topography used in our simulations is depicted in Figure 2 and leads to erroneous velocities smaller than 0.25 cm s^{-1} over most of the domain. The regions where numerical errors induce unrealistic features are pointed out in section 3.

Along the western (40°W), southern (30°N), and eastern (0.8°W) limits, original self-adapting open boundaries (OBs) evacuate the outgoing perturbations through radiation equations, and, in inflow regions, constrain the interior circulation by a strong relaxation of the baroclinic variables to a seasonal climatology. This lateral baroclinic climatology and the initial stratification come from the recent *T-S* climatology of *Reynaud et al.* [1998] (noted RLMB hereafter). These fields are based on several decades of hydrographic data and exhibit marked horizontal density gradients, thus providing the main incoming currents with a realistic location and baroclinic structure (especially along 40°W). Along these three OBs the vertically integrated flow (hereafter referred to as "barotropic" and denoted ψ), and consequently a large part of the lateral dynamical forcing, is adjusted to the interior dynamics by the model itself. This novel degree of freedom is a key element in our simulations. During model integration, along the northern "fixed" boundaries of the domain (66.5°N), the temperature, salinity, and baroclinic velocity fields were kept equal to their RLMB climatological seasonal estimates, and the barotropic stream function was prescribed to a linear profile between Greenland, Iceland and the northeastern corner. The reader is referred to P00 for a detailed description of the lateral forcing and of its impact on the interior solution. Table 1 and Table 2 summarize the parameters involved in this lateral forcing. The other model parameters, the buoyancy and mechanical surface forcings are presented in Table 3.

3. Annual Mean Circulation

P00 present the dynamical and thermodynamical adjustment of the basin and show that the annually averaged solution totally stabilizes after 35 years of integration. This is remarkable in the presence of such extensive self-adapting open boundaries. To complement the vector plots presented in P00, a scheme of the model mean circulation after 38 years of integration is shown in Figure 3 for three layers. The horizontal transports of individual currents indicated in this figure were computed across several zonal and meridional sections; the vertical transports were then deduced from the divergence of horizontal mass fluxes between these sections to close the mass budget. Figure 4 presents the annually and depth-averaged flow (ψ).

3.1. North Atlantic Current and the Subpolar Gyre

The NAC enters the domain between 43°N and about 53°N and crosses the MAR at 30°W between 44°N and 58°N. It brings 40.5 Sv above the MAR into the eastern basin (29.8 Sv, 7.4 Sv, and 3.3 Sv in the three depth ranges shown in Figure 3, respectively); most of this transport (29.8 Sv) is confined to the upper 800 m. The barotropic mass flux is significantly larger than the Sverdrup transport (Figure 5) across the same merid-

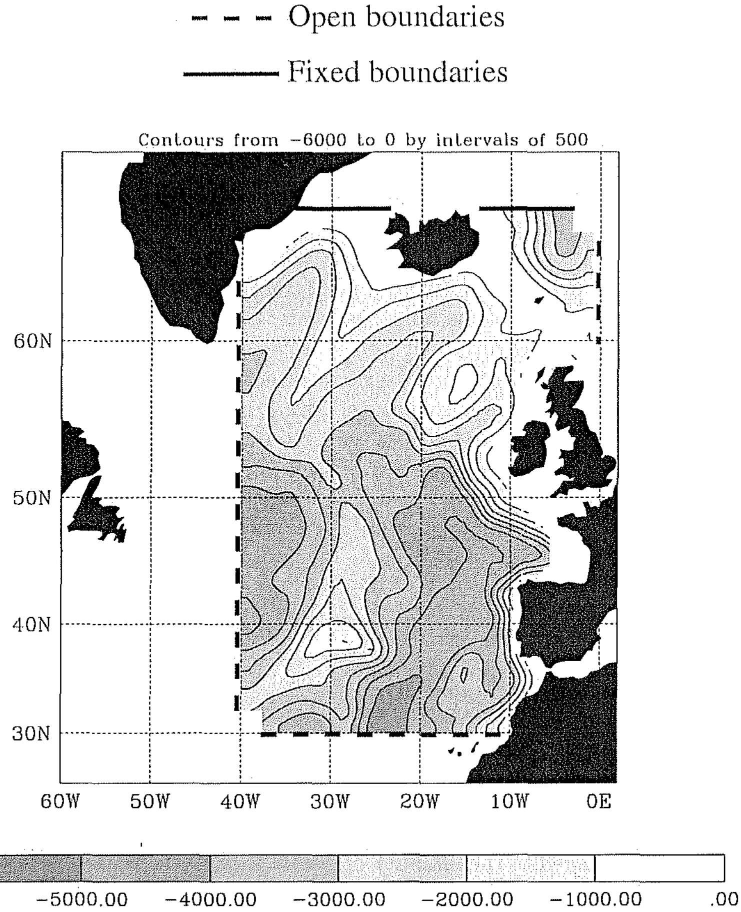

Figure 2. Model topography in meters. Plain lines locate the northern fixed boundaries where the model variables are prescribed; dashed lines locate the three self-adaptative open boundaries; unshaded three grid point square regions at the southwestern and northeastern corners correspond to artificial islands (necessary at the intersection of two open boundaries).

ian, suggesting that only two thirds of the NAC transport can be forced by the wind stress curl alone. The remaining third is likely to be due to current-topography interaction above the MAR, as was the case in the inversion by PM97.

Our estimate of the NAC transport above the MAR, like the inverse estimates of *Gana and Provost* [1993] and PM97 (58 and 48 Sv, respectively), significantly exceeds hydrography-based geostrophic estimates, which range between 16 Sv [*Wegner,* 1973] and 32 Sv [*Krauss et al.,* 1987]. Indeed, inverse and prognostic models represent the interaction of bottom currents with the topographic slopes, a process which is distorted or neglected in geostrophic computations when assuming the existence of a reference level at depth.

Table 1. Net Transports Prescribed Across The Domain Boundaries

Boundary	Net Transports, Sv
Western OB[a]	15 Sv eastward
Southern OB[a]	15 Sv southward
Eastern OB[a]	11 Sv eastward
Northwestern FB[b]	9 Sv southward
Northeastern FB[b]	2 Sv southward

[a]OB denotes a self-adapting open boundary. Along the OBs the profile of the barotropic stream function ψ is entirely diagnostic, without any relaxation.

[b]FB denotes a fixed boundary. Along the FBs the ψ profile is set equal to a fixed linear profile.

Figure 3 shows that the NAC is deflected northeastward at all depths above the MAR, as suggested by *Sy* [1988, Figure 11], but more markedly than in certain other studies [PM97; *Otto and van Aken,* 1996]. This steering is associated with a local maximum of the vertical stretching within the Charlie Gibbs Fracture Zone (CGFZ), where the bottom flow is downslope and eastward. The westward bottom flow observed in this passage [*Saunders,* 1994] is not reproduced by the model probably because the local vertical resolution (about 500 m near the bottom) is too weak for a correct representation of the vertical shear of horizontal velocities.

Figure 3 shows that downstream of the MAR, two branches of the NAC flow toward the subpolar gyre and the Norwegian Sea along the northern and southern flanks of the Rockall Plateau:

Table 2. Timescales τ Used Along the Western, Eastern, and Southern Self-Adapting Open Boundaries (OBs) for the Relaxation of the Model Baroclinic Variables to Climatology[a]

Model Variable	τ in Outflow Regime	τ in Inflow Regime
Temperature, salinity	5 years	15 days
Baroclinic normal velocity	5 years	3 days
Total tangential velocity	5 years	3 days

[a]Climatological values for the tracers come from the seasonal climatology of *Reynaud et al.* [1998] (noted RLMB); climatological values for the baroclinic normal velocity field geostrophically derive from the RLMB density fields (their depth-averaged component is removed at each point of the boundary); the climatological value for the total tangential velocity field is zero. In addition to this relaxation, outgoing barotropic and baroclinic perturbations are radiated away through the OBs. The barotropic stream function ψ is never relaxed to any climatological profile along the OBs; that is, $\tau_\psi = \infty$ at each time step and each grid point in outflow and in inflow regimes.

1. A 17.7-Sv branch of the NAC crosses 20°W toward the Rockall Trough. It has a strong vertical shear since 93% of its transport is confined to the upper 800 m (Figure 3a). Within the Rockall Trough, 0.9 Sv of this transport are downwelled below 1500 m and join the subtropical area. The remaining part (16.8 Sv, close to the 14-Sv estimate of *McCartney and Talley* [1984]) finally exits the Rockall Trough between the Rockall Plateau and Scotland.

2. The northernmost branch of the NAC brings 12.2 Sv from the MAR across 20°W toward the eastern Iceland Basin. This branch is more barotropic than the previous one since 55% of its transport (6.8 Sv, Figure 3a) is found above 800 m.

Table 3. Model Parameters and Surface Forcing

Model Parameter	Value
	Spatial and Temporal Resolution
Horizontal resolution Δ	isotropic, $\Delta = 0.8°$ in longitude, $0.8° \times \cos(\phi)$ in latitude ϕ: Δ=77 km at 30°N, Δ=35 km at 66.5°N.
Vertical resolution Δ_Z	21 sigma levels, Δ_Z ranges from 11 m to 28 m near the surface, from 48 m to 671 m near the bottom
Time step	1 hour
	Parametrization of Subgrid Scale Processes
Bottom friction	linear law; the coefficient is 2.65×10^{-4} s^{-1}
Horizontal turbulent viscosity	$3000 \times \Delta/\Delta_{max}$ m^2 s^{-1} (laplacian operator)
Horizontal turbulent diffusivity	$875 \times \Delta/\Delta_{max}$ m^2 s^{-1} (laplacian operator)
Vertical turbulent viscosity	10^{-4} m^2 s^{-1} (10^{-3} in the top 50 m)
Vertical turbulent diffusivity	10^{-4} m^2 s^{-1} (10^{-3} in the top 50 m)
In case of static instability	the vertical diffusivity is set to 1 m^2 s^{-1}, and a convective adjustment is made every day where necessary
	Surface Forcing[a]*, Applied as a Body Force on the Top 50 m*
Heat flux	monthly ECMWF[b] heat flux with a relaxation of the sea surface temperature to seasonal RLMB[c] values
Salt flux	relaxation of the sea surface salinity to seasonal RLMB[c] values
Wind stress	*Hellermann and Rosenstein* [1983] monthly climatology
	Parametrization of the Mediterranean Water Overflow
Relaxation timescale of tracers	30 days in the Gulf of Cadiz at all depths to RLMB[c] seasonal values; Gibraltar Straits is closed

[a]This surface forcing is adapted from *Barnier et al.* [1995].
[b]ECMWF refers to the European Centre for Medium-Range Weather Forecasts.
[c]RLMB refers to *Reynaud et al.*'s [1998] *T-S* seasonal climatology.

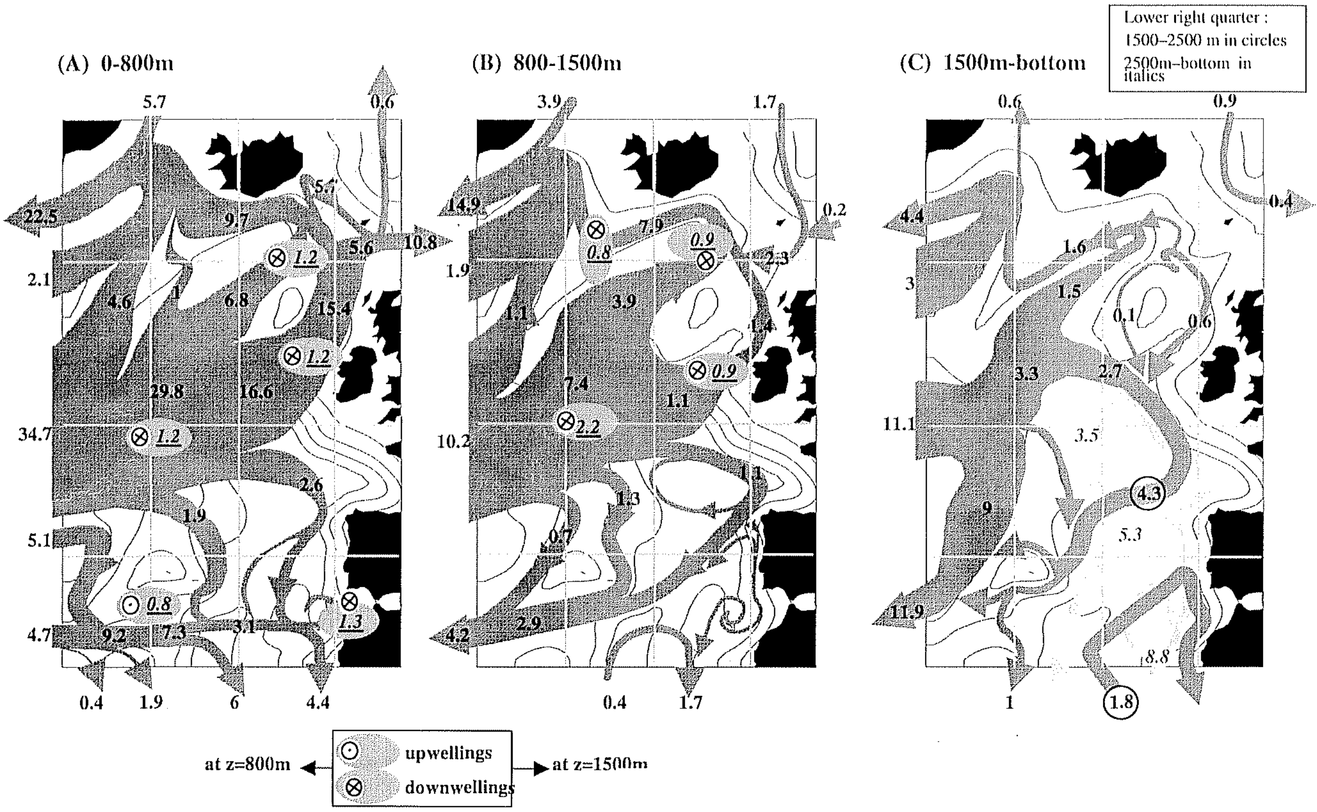

Figure 3. Scheme of the model circulation showing the horizontal transports (Sv) in three different layers: (a) 0-800 m including the Ekman transport; (b) 800-1500 m; and (c) 1500 m to bottom. In the lower-right quadran of Figure 3c, light shaded arrows and numbers in italics represent the horizontal circulation between 2500 m and the bottom, whereas dark gray arrows and circled numbers correspond to the horizontal circulation between 1500 and 2500 m. Everywhere else in Figure 3c, currents are vertically more coherent: numbers correspond to horizontal transports between 1500 m and the bottom. Vertical transports between the layers are underlined (in Sv), and close the local volume budgets; arrows are drawn where the vertical transports are maximum. Horizontal and vertical straight lines are drawn every ten degrees of longitude and latitude starting from (40°W, 30°N) in the southwestern corner.

Therefore 72% (16.8 + 12.2 Sv) of the NAC transport above the MAR (40.5 Sv) circulates northward; this result is close to that of PM97. A 11.3-Sv warm Atlantic water flow enters the Norwegian Sea above the Iceland-Scotland Ridge (ISR) within two branches of similar intensity (5.6 and 5.7 Sv, Figure 3a). This total surface flow toward the Norwegian Sea is about 30% stronger than the estimate of *Orvik et al.* [1999]. The westward transport of Iceland-Scotland Overflow Water (ISOW, $\sigma_0 > 27.8$) above the ISR sill was estimated to be 2.7 Sv by *Dickson and Brown* [1994]. In the model this transport depends on the section considered, since a strong entrainment exists in this area, and ranges between 2.3 Sv and 3.5 Sv. As in the circulation scheme proposed by these authors, the model ISOW then spreads into the Rockall Trough and along the ISR western flank, recirculating mainly within the subpolar gyre.

The depth-integrated westward transport south of Iceland reaches 31 Sv according to *Schmitz and McCartney* [1993]). Figure 4 shows that this mass flux amounts to 21 Sv in the model: 19.2 Sv (9.7 Sv, 7.9 Sv, and 1.6 Sv in the three layers shown in Figure 3) flow along the topographic slope and are intensified by a 1.8 Sv recirculation centered around (25°W, 60°N) visible in Figure 4.

The Irminger Current enters the model domain by the western boundary near 60°N; its depth-averaged transport is then 7 Sv with a significant contribution from all layers (Figure 3). It is later augmented by the contribution of a branch from the northern NAC which does not enter the eastern basin. This increases the northward transport to 12.7 Sv west of the Reykjanes Ridge. The Irminger Current circulates cyclonically and meets the East Greenland Current (EGC). The 9-Sv southward flow prescribed through the Denmark Strait finally intensifies the EGC transport up to 41.8 Sv. This value was not constrained a priori, but is similar to *Schmitz and McCartney*'s [1993] estimate. The model solution in the subpolar gyre is also very close to the circulation scheme of *Otto and van Aken* [1996], derived from drifter data.

3.2. Intergyre Zone and the Subtropical Gyre

East of the MAR the southward recirculating branches of the NAC bring 11.2 Sv of water toward the subtropical gyre across the intergyre zone. This flow is

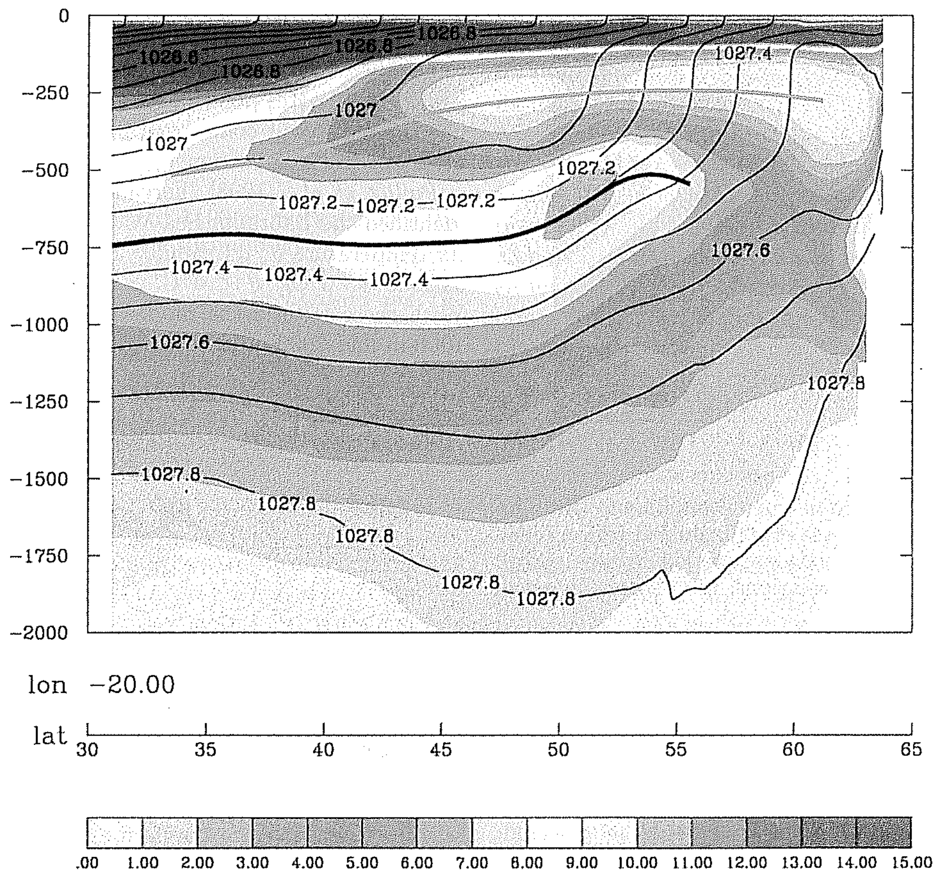

Plate 1. Mean large-scale potential vorticity (PV equal to $-f\rho_z$) and density fields averaged between 24°W and 16°W. The thick blue line locates the PV minimum associated with the core of SPWM; the thick black line locates the PV maximum associated with the main thermocline.

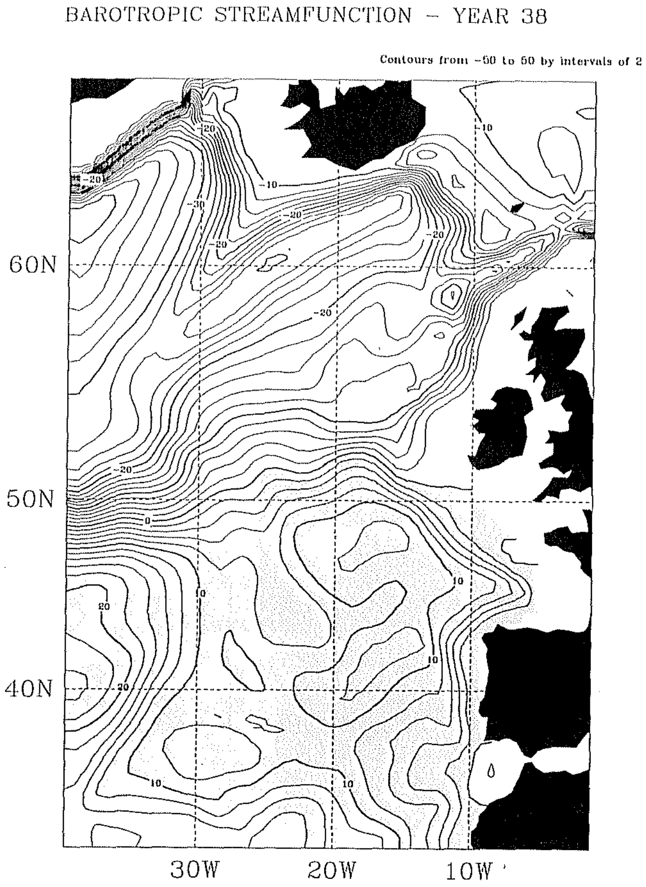

Figure 4. Mean barotropic stream function ψ (Sv). In this and subsequent Figures of ψ, unshaded regions correspond to cyclonic circulations, shaded regions correspond to anticyclonic circulations; the contour interval is 2 Sv.

distributed over the three layers of Figure 3: 1.9 + 2.6 Sv, 1.3 + 1.1 Sv, and 4.3 Sv from top to bottom. Like the PM97 circulation scheme, our solution above 800 m shows the southern limit of the subpolar gyre to lie largely south (around 47°N) of what would be expected without topographic forcing (i.e., the zero contour in Figure 5). Between 40°N and 50°N, about 1.75 Sv of Subpolar Mode Water (SPMW) are subducted into the ocean thermocline [*Penduff,* 1998]; with the same method, PM97 obtain a similar subduction rate (2.5 Sv).

The subtropical gyre is also fed from the west above 800 m by the Azores Current (AC), rarely simulated by coarse-resolution models. The AC brings 9.2 Sv eastward across 35°W between 30°N and 35°N, is fed from the north all along its eastward path by the southward flow of thermocline waters (4.5 Sv), and loses 8.3 Sv southward between the MAR and 20°W (Figure 3a). The AC intensity thus decreases downstream, and only 4.4 Sv leave the domain through the southern boundary east of 20°W. These features are remarkably coherent with the results of *Stramma* [1984] and *Klein and Siedler* [1989], and with the circulation scheme of *Siedler and Onken* [1996, Figure 11.6].

At intermediate levels, salinity exceeds S = 36.01 in the northern Gulf of Cadiz (Figure 6). The northwestern limit (defined as S = 35.11 at 1100 m as in the work of *Richardson and Tychensky* [1998]) of the Mediterranean Water (MW) tongue is positioned correctly, despite the crude representation of the Mediterranean Water (MW) salt source and the modest resolution of the model which probably explain the partial erosion of the salinity horizontal gradient. A cyclonic circulation surrounds the MW tongue (Figure 3b). A similar tendency is described by *Reid* [1994], and deduced by *Schmitz and McCartney* [1993] with a level of no motion below the MW (as in the present solution, see section 4). However, results from *Saunders* [1982] and *Maillard* [1986] contradict this picture. Within the MW, north of about 35°N, these authors report a poleward flow which was rationalized by *Schopp and Arhan* [1986]. This latter point of view appears more convincing to us; we will come back to this deficiency of the model in the next section.

Paillet et al. [1998] (hereafter reffered to as P98) identified the Labrador Sea Water (LSW) at 35°W by its temperature θ, its salinity S, and its immersion z as follows: 3°C< θ < 4°C, S < 34.94, z > 1000 m. With these criteria the model LSW is found between 1000 m and 2000 m in this region at locations close to

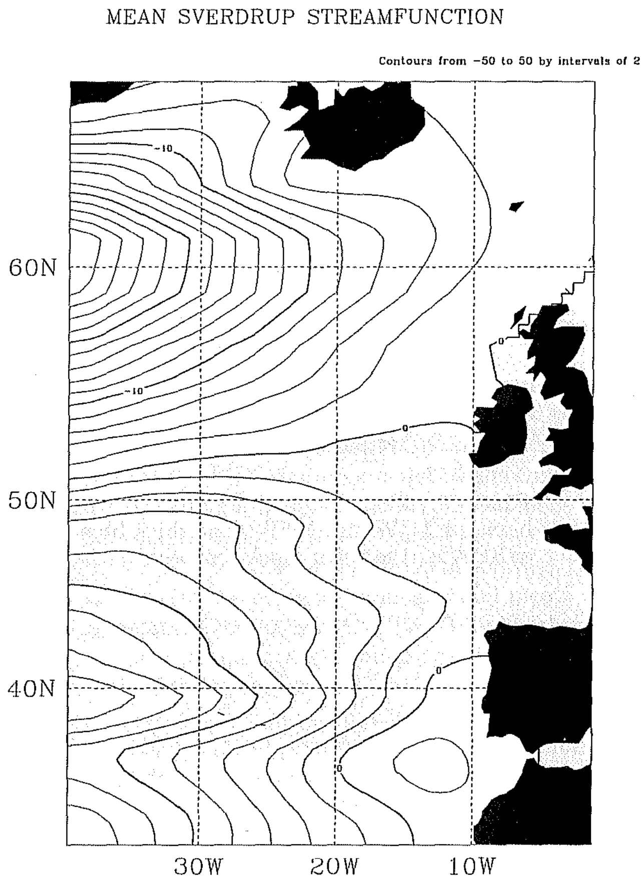

Figure 5. Sverdrup barotropic stream function (Sv), given by the westward integration of the wind stress curl from *Hellermann and Rosenstein*'s [1983] annual climatology. Contour interval is 2 Sv.

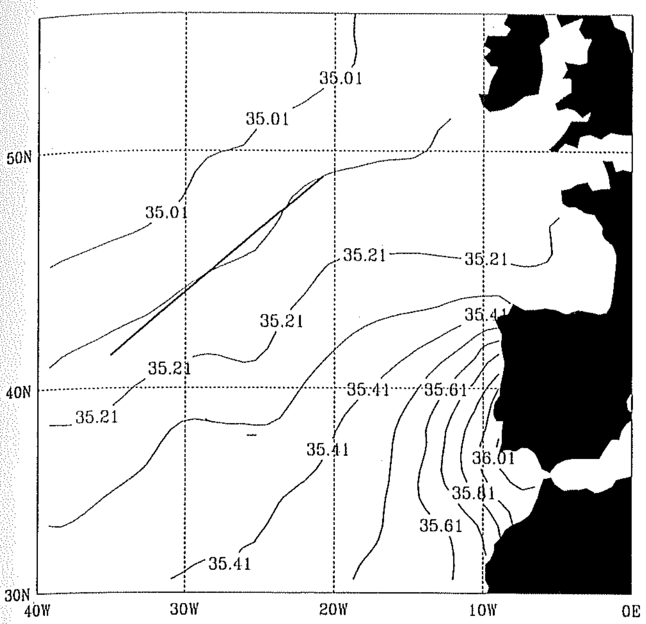

Figure 6. Model salinity at 1100 m averaged over the last year of integration. The surimposed segment is fitted to the northern limit of the Mediterrannean Water tongue (contour 35.11) as shown in *Richardson and Tychensky* [1998, Plate 4].

those deduced from the RLMB climatology. The NAC system advects 4.9 Sv of LSW across 35°W to the east, i.e., 22% less than estimated by P98. This LSW flow then splits into three main branches (Figure 3c): Using the local criteria chosen by P98, 1.4 Sv of LSW (1.5 Sv according to P98) flow toward the Subpolar Gyre across 54°N; a second branch follows the eastern flank of the MAR southward with local recirculations toward the western basin, and finally flows around the Azores Plateau; the third branch goes across the eastern basin, steers southeastward and passes to the south of the Azores. The model concentrates this third branch along the Porcupine Bank north of 48°N. This feature appears unrealistic and due to the use of sigma coordinates since it is also observed in the resting stratification case. *Knochel* [1998] reports a similar tendency in a coarse-grid North Atlantic configuration of SPEM; his results suggest that a significant increase (almost double) in the vertical resolution would correct this discrepancy. When LSW is identified with the same local criteria as P98 across 44°N (2.8°C< θ < 4°C, S < 35), the southward transport of LSW between 35°W and the coast is 6.9 Sv (i.e., 44% more than in P98), of which 1.5 Sv (i.e., 50% less than P98) flows east of the MAR. The afromentioned local recirculations of LSW toward the western basin are probably favored by the deepening of the MAR consecutive to topographic smoothing and probably contributes to the weak southward flow of LSW in the eastern basin. It should be mentioned that model LSW transports are very sensitive to small changes in temperature and salinity ranges, especially along 35°W and 44°N. In addition, the way LSW characteristics evolve by mixing between these sections depends on the model formulation and parameters. These two reasons explain why P98's local criteria do not lead here to a closed mass budget for the LSW. When modeled LSW transports are considered individually, their agreement with P98 are thus modest at 44°N, good at 35°W, and excellent at 54°N.

A 1.8-Sv southward flow is simulated by the model between 1500 and 2500 m south of 39°N along the eastern boundary. It is associated with an anticyclone centered around (15°W-32°N) near the southern open boundary. This along-shelf southward flow is also present in P97 and is probably unrealistic.

Below 2500 m in the subtropical gyre the model drives a 3.5 Sv to 8.8 Sv deep anticyclonic circulation. It is depicted by the dark loop in Figure 3c and has a signature on ψ along the coast of Europe (Figure 4). This circulation is opposite to that observed by *Dickson et al.* [1985], and may be due to the use of sigma coordinates since a southward flow along the coast of Portugal is also visible in the resting stratification case, and in coarse- and fine-grid North Atlantic configurations of SPEM [*Knochel*, 1998; *DYNAMO Group*, 1997]. In the present regional configuration, in particular, this discrepancy at depth can hardly be compensated for by either the largely passive self-adapting southern open boundary or the surface forcing which mainly affects the layers located above the marked thermocline.

3.3. Zonally Averaged Circulation in the Intergyre Zone

By way of an introduction to section 4, the zonally and annually averaged model meridional velocity field is presented at different latitudes in Figure 7. Below the ageostrophic surface Ekman layer this figure may be compared with the zonally averaged absolute geostrophic velocity field estimated from hydrography by *Saunders* [1982] (Figure 7b) at the same latitudes, under the assumption of a Sverdrupian barotropic flow. Since the geostrophic balance and the Sverdrupian nature of the depth-integrated flow may be affected by ageostrophic currents and topographic effects along the eastern boundary and since the model results exhibit a few discrepancies along the coast, we chose a band of zonal averaging (24°W-16°W) narrower than that considered by Saunders (from the MAR to the eastern boundary). Our estimate is still representative of the large-scale circulation in the eastern basin can be compared to the estimate by Saunders.

Between 48°N and 30°N the southward advection of Central Waters and SPMW by the NAC recirculation is well simulated within a surface layer that thickens southward (from 300 to 800 m). North of 45°N, below this surface current, denser SPMW flows northward within a layer that thickens progressively, as estimated by *Saunders* [1982].

Around 1000 m within the tongue of MW the model meridional flow is weak at all latitudes; it is oriented southward at 36°N and 41.5°N and northward north of about 45°N. *Saunders* [1982] reports a poleward flow at this latitude, but also at 41.5°N. This model discrepancy may be related to the crude representation of the MW overflow in the Gulf of Cadiz. The parametriza-

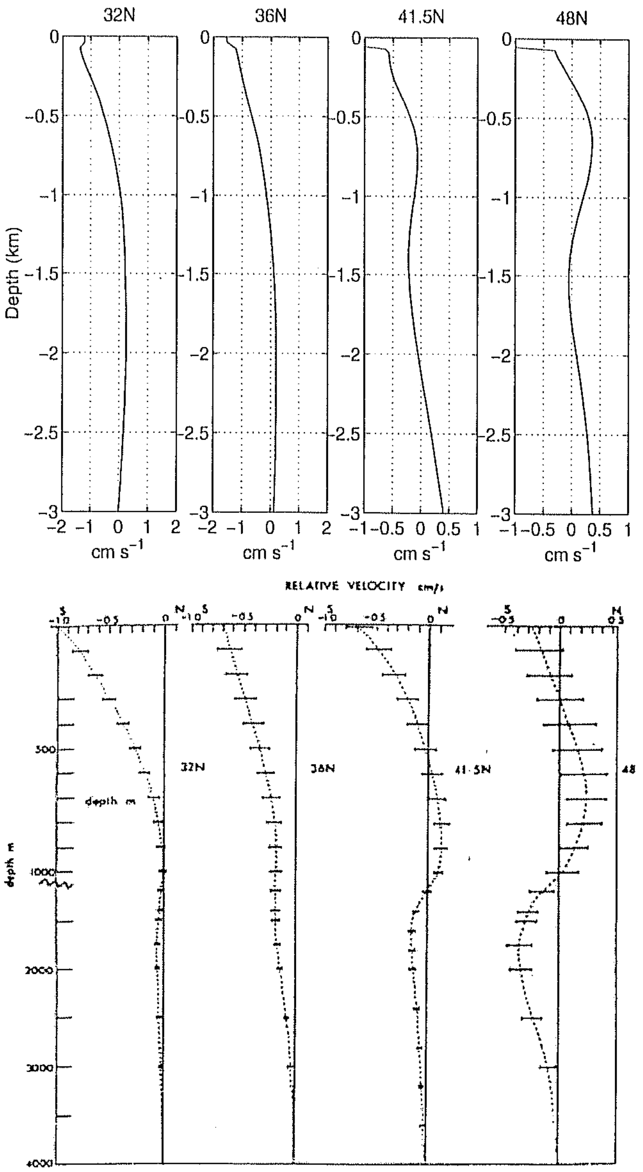

Figure 7. (top) Model meridional velocity (in 10^{-2} m s^{-1}) at four latitudes in the model, averaged over the last year of integration and between 24°W and 16°W. (bottom) Mean geostrophic velocity (in 10^{-2} m s^{-1}) east of the Mid-Atlantic Ridge at the same latitudes, computed by *Saunders* [1982] from in situ data with a reference level at 4000 m. Note the change of vertical scale at 1000 m.

tion of the MW source term by a simple *T-S* relaxation, the presence of a closed boundary at the strait, the absence of important topographic details and steep slopes in the smoothed bathymetry, and the modest horizontal resolution are likely to distort the local dynamics (in particular, the exxagerated width of the northward flowing MW vein along the coast of Portugal) and the large-scale circulation within the MW intrusion at this latitude. Another explanation will be proposed below.

The southward flow of LSW presented in the previous section is visible at 41.5°N in Figure 7 below 1500 m but not farther south because the flow is confined along the eastern flank of the MAR, outside the longitude band of averaging. The northward flow that appears at 36°N and 32°N is associated with the western part of the 2.8-Sv anticyclone mentioned previously between 1500 and 2500 m.

The northward flow visible below 2500 m in Figure 7a corresponds to the western part of the deep basin-wide anticyclone mentioned earlier (Figure 3c). Contrary to what Figure 7a suggests, this unrealistic model feature does not induce any net meridional transport in the deep eastern basin since the region of the European shelf, along which the southward return flow is confined, is excluded from the band of longitudinal averaging.

4. Dynamics and Thermodynamics of the Intergyre Zone

The mean circulation in the band 24°W-16°W is now investigated within four potential density layers (Table 4) which are representative of SPMW and MW in the intergyre zone. The mean density field is shown in Plate 1. The isopycnal surfaces 26.9, 27.1, and 27.4 lie above, along, and below, respectively, the potential vorticity minimum associated with the core of SPMW. The isopycnal surfaces 27.6 and 27.8 lie approximately within and below the MW, respectively.

In a non diffusive adiabatic ocean, diapycnal velocities are zero, and the flow is parallel to isopycnal surfaces. This hypothesis underlies the theory of the ventilated thermocline [*Luyten et al.,* 1983] which has often been used to investigate the large-scale dynamics of this particular region [*Schopp and Arhan,* 1986; *Paillet and Arhan,* 1996]. However, in the real ocean, turbulent diffusion (parameterized in our model by laplacian operators in the vertical and the horizontal) is expected to induce mass exchanges between density layers, and may generate meridional motions in these layers through vortex stretching. Our computations concerning both

Table 4. Density Range and Water Mass Embedded Within Each of the Four Isopycnal Layers Considered in Section 4

Layer	Density Range	Water Mass
1	$26.9 < \sigma_0 < 27.1$	upper Subpolar Mode Water
2	$27.1 < \sigma_0 < 27.4$	lower Subpolar Mode Water
3	$27.4 < \sigma_0 < 27.6$	upper Mediterranean Water
4	$27.6 < \sigma_0 < 27.8$	lower Mediterranean Water

processes are explained in section 4.1; the dynamical impact of vertical and horizontal diffusion is presented in section 4.2; the importance of diapycnal transfers with respect to the adiabatic part of the flow is discussed in section 4.3.

4.1. Diagnostics

4.1.1. Buoyancy balance. The density equation may be written as follows (subscripts t and z denote the temporal and vertical partial derivatives):

$$\rho_t + \underline{u}^h.\nabla\rho + w.\rho_z = K_v\rho_{zz} + K_h\nabla^2\rho + S, \qquad (1)$$

where ρ, $\underline{u}^h$, w, K_v, K_h, and S denote the density field, the horizontal and vertical velocity fields, the vertical and horizontal diffusion coefficients, and the surface density fluxes, respectively. Since the annually averaged stratification is stable and since the vertical coordinate z increases upward, ρ_z is negative everywhere.

In the following sections, we shall focus on the mean state of the ocean interior, which is not directly affected by atmospheric fluxes S, nor by convective events. The first and last terms in equation (1) will thus be neglected and our investigations restricted to south of about 50°N. Away from convection regions, after a temporal averaging, equation (1) provides the following expression for the annual mean vertical velocity field w:

$$w = \overbrace{-\frac{1}{\rho_z}\underline{u}^h.\nabla\rho}^{w_i} + \overbrace{\underbrace{\frac{1}{\rho_z}K_v\rho_{zz}}_{w_{cV}} + \underbrace{\frac{1}{\rho_z}K_h\nabla^2\rho}_{w_{cH}}}^{w_c}. \qquad (2)$$

In this equation, w is expressed as the sum of its isopycnal (w_i) and diapycnal (w_c) components. Diapycnal velocities w_c can be induced by vertical and horizontal diffusion, the respective contributions of which are denoted by w_{cV} and w_{cH}. Along a steady isopycnal surface a positive value of w_{cV} (w_{cH}, respectively) means that vertical (horizontal, respectively) diffusion induces an upward transport across the surface which tends to inflate the lighter layer located above the isopycnal at the expense of the heavier one located below, and therefore to decrease the density averaged over this pair of layers. Since the annually averaged density field is almost steady, such a trend in the density equation (2) must be compensated for by other terms. Despite the fact that the values of K_v and K_h are set by numerical stability requirements and may be overestimated in the model, and that some processes known to induce diapycnal mass transfers (like double diffusion below the MW intrusion [*Arhan*, 1987; *Paillet et al.*, 1998]) are not taken into account, our annually averaged numerical solution may provide information about the origin and the effect of w_{cV} and w_{cH} on the meridional circulation in the intergyre zone.

The model vertical velocity w was deduced from the annually averaged horizontal flow using SPEM's original continuity equation. The terms w_i, w_{cV}, and w_{cH} were computed from the annual mean density and velocity fields, and from the local values of K_v and K_h according to their individual expressions given in equation (2). The terms w, w_i, w_{cV}, and w_{cH} were then interpolated and smoothed along the five selected isopycnal surfaces, and averaged between 24°W and 16°W.

The balance in equation (2) cannot be verified perfectly in the model solution because surface fluxes force convective mixing down to a certain level, because of the averaging and interpolating errors, and because T and S trends may persist. The maximum residual vertical velocity tolerated in equation (2) was arbitrarily set to $w_{\text{lim}} = 2 \times 10^{-7}$ m s^{-1}. During the 38th year of integration the temperature trend in the subtropical gyre is about 2.5×10^{-3} °C per year above 1000 m and 5 times smaller below 1000 m (see P00). Taking typical values of ρ_z from Plate 1 (10^{-3} °C m^{-1} and 5×10^{-4} °C m^{-1} above and below 1000 m) and a thermal expansion coefficient of about -2×10^{-4} (°C)$^{-1}$ shows that this thermal drift induces in equation (2) an imbalance smaller than 2×10^{-8} m s^{-1} above 1000 m and 2.5 smaller below that depth. The errors induced by the salinity drift, computed with a haline contraction coefficient of 8×10^{-4} are several orders of magnitude smaller than those due to the thermal drift. These errors are clearly smaller than w_{lim}: the imbalance in equation (2) is expected to be due to convective events and/or to the interpolation procedure rather than to temperature and salinity drifts.

Figure 8 highlights the regions where our results can be interpreted, i.e., where the residual in equation (2) (the departure between w_c and $w - w_i$) is smaller than w_{lim}. In Figures 8 and 9, thick lines indicate where this criterion is verified. Equation (2) appears to be more correct along the three upper isopycnal surfaces than along the other two (the model dynamics in isopycnal layers 3 and 4 will thus be interpreted with caution), but some large-scale trends make sense everywhere. Figure 9 presents the meridional profiles of w_{cV} and w_{cH} along the five selected isopycnal surfaces.

4.1.2. Vorticity balance. In the isopycnal layers of Table 4 we shall investigate how the model mean meridional circulation, averaged between 24°W and 16°W, is influenced by the different components of vertical stretching. Let us consider an isopycnal layer of local thickness Δz, and let V_p denote the layer-averaged local meridional circulation induced by vortex stretching. It is proportional to Δw, the vertical velocity difference between the upper and lower limits of the layer:

$$V_p = \frac{f}{\beta}\frac{\Delta w}{\Delta z}, \qquad (3)$$

where f and β denote the Coriolis parameter and its meridional gradient respectively. V_p was computed from the actual model vertical velocity w interpolated along the isopycnals given in Table 4. Figure 10 presents V and V_p. Thick lines in this figure locate the areas where the following conditions are fullfilled in a given isopycnal layer: $|w| < w_{\text{lim}}$ along its upper and lower limits, and the large-scale trends of V are similar to those driven by vortex stretching (V_p). There the large-scale flow is mainly controlled by geostrophy. Substituting (2) in (3) gives the following expression for V_p:

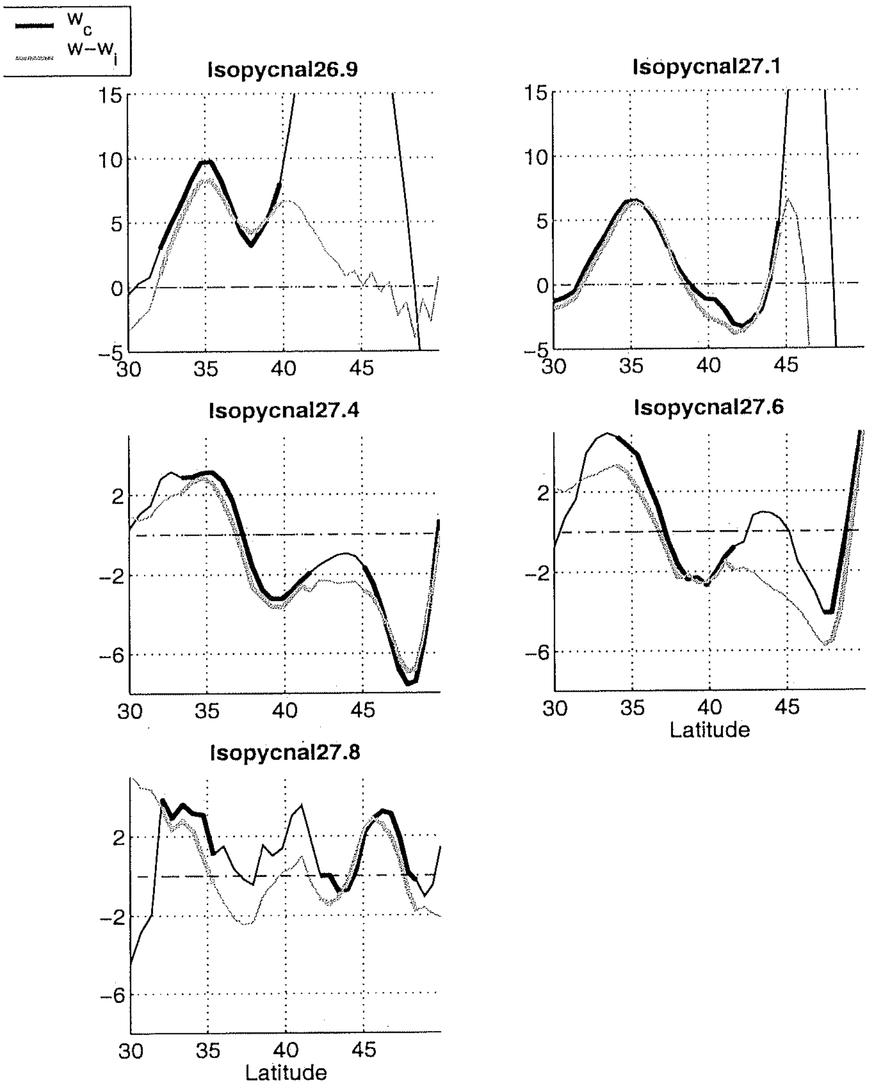

Figure 8. The balance between w_c and $w - w_i$ (10^{-7} m s^{-1}) along the isopycnal surfaces 26.9, 27.1, 27.4, 27.6, and 27.8. Thick segments indicate the regions where the two terms differ by less than 2.10^{-7} m s^{-1} and where equation (2) will thus be considered as correctly valid. Both quantities have been averaged in the band 24°W - 16°W.

$$\underbrace{V_p}_{\frac{f}{\beta}\frac{\Delta w}{\Delta z}} = \underbrace{V_{pi}}_{\frac{f}{\beta}\frac{\Delta w_i}{\Delta z}} + \underbrace{V_{pV}}_{\frac{f}{\beta}\frac{\Delta w_{cV}}{\Delta z}} + \underbrace{V_{pH}}_{\frac{f}{\beta}\frac{\Delta w_{cH}}{\Delta z}} . \quad (4)$$

V_{pi}, V_{pV}, and V_{pH} (shown in Figure 11 along with V) denote the meridional velocities driven by the vertical stretching of w_i, w_{cV}, and w_{cH}, respectively, and where computed individually as written in the previous equation. Thick lines in Figure 11 were deduced from those in the previous figure, with the additional constraint that in equation (4) the absolute value of the leading term must be superior to 3 times the residual. Equation (4) will be considered as valid in regions denoted by thick lines in Figure 11.

4.2. Dynamical Impact of Diffusion

The contributions of vertical and horizontal diffusion to the buoyancy balance (w_{cV} and w_{cH}, respectively) are shown in Figure 9 for each of the five selected isopycnal surfaces.

4.2.1. Vertical diffusion. The meridional circulation V_{pV} driven through vortex stretching by vertical diffusion is shown along with the actual meridional velocity V in Figure 11 for the four isopycnal layers.

4.2.1.1. Layer 1: Along the isopycnal surface 26.9, located below the surface stratification south of 40°N, ρ_{zz} is negative. Since ρ_z is also negative, vertical diffusion induces an upward diapycnal velocity w_{cV} (Figure 9). Since w_{cV} is weaker along the isopycnal surface 27.1, vertical diffusion induces stretching in layer 1 and therefore a northward motion within the upper SPMW (Figure 11). The strong w_{cV} maximum visible in Figure 9 between 40°N and 48°N along the uppermost isopycnal surface is due to the vertical penetration through vertical diffusion of the atmospheric buoyancy input (S is important here). Since the residual in equation (2) largely exceeds w_{lim}, we will not interpret this feature further.

4.2.1.2. Layer 2: The isopycnal surface 27.1 lies near the potential vorticity minimum associated with the subducted SPMW south of 40°N, but is located underneath it north of 40°N (Plate 1). The diapycnal velocity w_{cV}, which is negatively correlated with ρ_{zz}, is thus weak south of 40°N and negative further north (Figure 9). South of 40°N, w_{cV} does not differ much along the upper and lower limits of layer 2 (isopycnal surfaces 27.1 and 27.4 in Figure 9). Vertical diffusion thus induces no significant meridional motion V_{pV} within the dense SPMW (Figure 11). North of 40°N in layer 2, vertical diffusion shrinks layer 2 and drives a southward motion.

4.2.1.3. Layers 3 and 4: Below the main thermocline along the isopycnal surfaces 27.4, 27.6, and 27.8, ρ_z and ρ_{zz} are negative. Vertical diffusion thus induces a positive diapycnal velocity w_{cV} across these surfaces (Figure 9), in accordance with the classical theory of *Stommel and Arons* [1960]. Since ρ_z tends to zero downward, w_{cV} increases downward: through vortex stretching, vertical diffusion induces an equatorward flow within the upper MW between 35°N and 42°N (V_{pV} in Figure 11, layer 3). Despite the noisy character of our computations in layer 4, Figure 11 suggests that the same process drives a southward motion of in the lower part of the MW extension in the same latitude range.

To summarize, vertical diffusion induces a rather simple baroclinic meridional circulation V_{pV} through vortex stretching in the intergyre zone (except north of 40°N in the upper and lower SPMW where the situation is more complex): A poleward flow opposite to the mean advection (see V in Figure 10) within layer 1 that vanishes in layer 2; an equatorward flow below, like V, suggesting that the southward advection within the upper and lower parts of the MW tongue is promoted by vertical diffusion.

4.2.2. Horizontal diffusion. The diapycnal velocity field and subsequent meridional motions induced by horizontal diffusion (w_{cH} in Figure 9 and V_{pH} in Figure 11) exhibit a different structure. We first describe their large-scale characteristics, and then briefly present their content at smaller scales.

4.2.2.1. Large-scale tendencies: Along the isopycnal surfaces 27.1 and 27.4 which constitute the upper and lower limits of layer 2 (dense SPMW), w_{cH} exhibits opposite large-scale meridional gradients (positive along 27.1 and negative along 27.4), related to the curva-

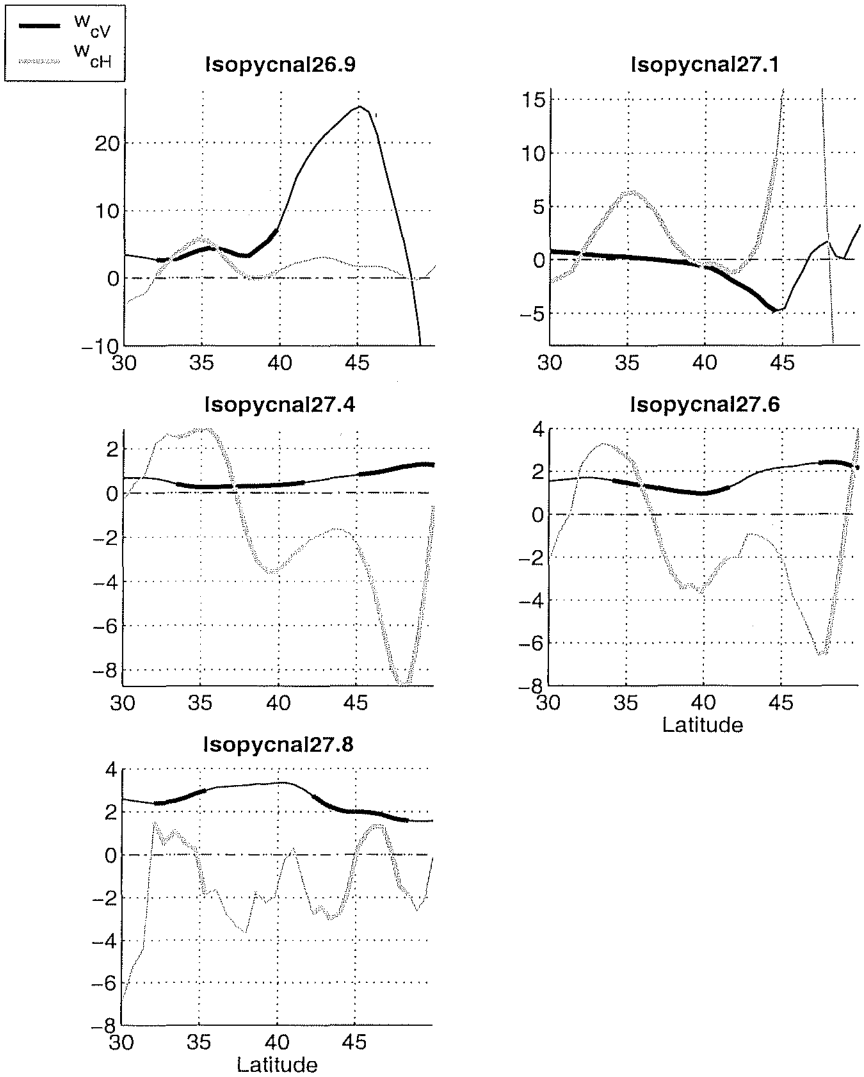

Figure 9. The two components of w_c (in 10^{-7} m s^{-1}), averaged between 24°W and 16°W, along the isopycnal surfaces 26.9, 27.1, 27.4, 27.6, and 27.8. Thick lines as in Figure 8.

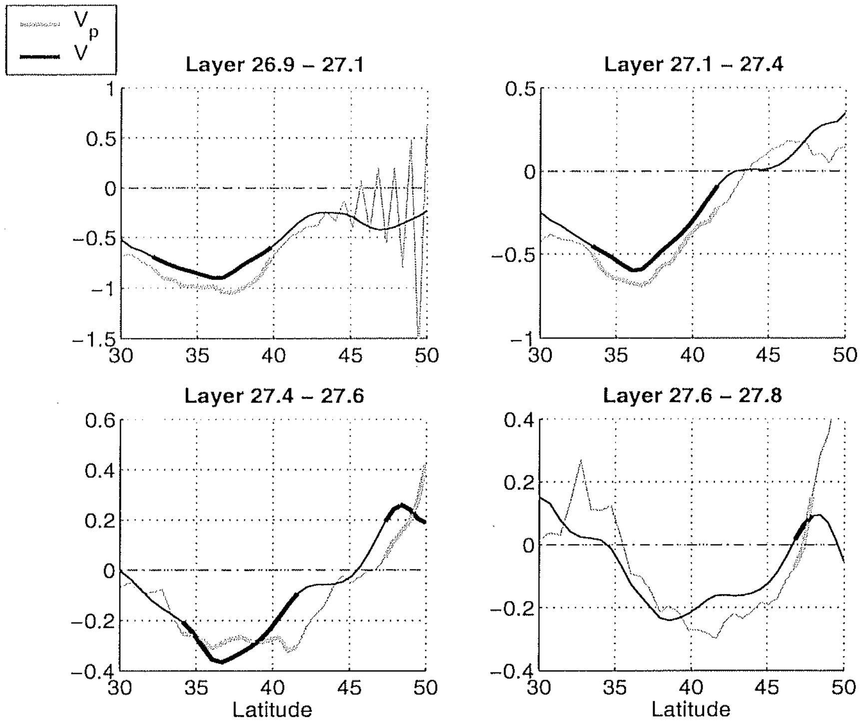

Figure 10. Meridional velocity V_p driven by vertical stretching Δw, and model mean meridional velocity V (in 10^{-2} m s^{-1}). Both terms are averaged between 24°W and 16°W and within the four isopycnal layers of Table 4. Lines are thickened where equation (2) has been validated along the upper and along the lower interfaces of each layer and where V is similar to V_p.

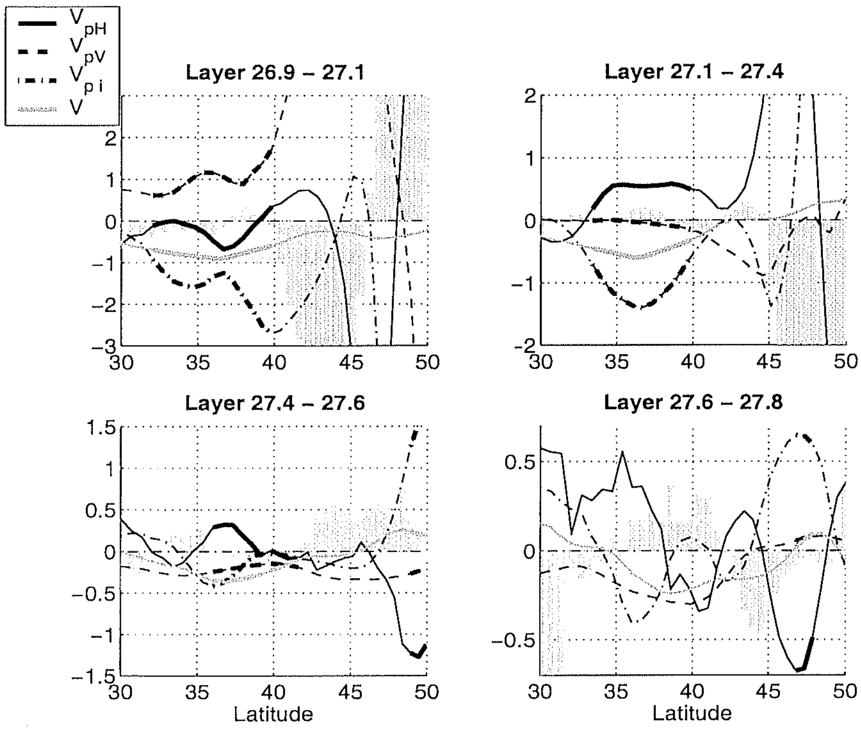

Figure 11. The three components of V_p, along with the model meridional velocity V (in 10^{-2} m s^{-1}). These terms are averaged annually, between 24°W and 16°W, and within the four isopycnal layers of Table 4. Gray bars show the residual r in equation 4. Thick lines in this figure have been deduced from those in Figure 10 (criterion 1) with a restriction to the areas where r is smaller than the dominant terms in equation 4 (criterion 2). Both criteria appear to be fulfilled at the same time in most regions. The dynamical analysis presented in the text focuses on thick lines.

ture of isopycnal surfaces. Between 33°N and 42°N within the lower SPMW the subsequent vertical stretching thus induces a northward motion which counteracts the equatorward motion of dense SPMW simulated by the model (V_{pH} and V in Figure 11). Along the isopycnal surfaces 27.4 and 27.6, w_{cH} decreases northward in a similar fashion indicating that horizontal diffusion does not drive any large-scale meridional circulation through vortex stretching in the upper MW (Figure 11). However, w_{cH} exhibits no large-scale meridional gradient along the isopycnal surface 27.8. In layer 4 (lower MW), horizontal diffusion is likely to contribute to the simulated equatorward flow V north of about 40°N and to oppose it south of 40°N.

4.2.2.2. Smaller scales: The diapycnal velocity w_{cH} induced by horizontal diffusion also varies at scales of about 600 km. Figure 9 shows a regular succession of w_{cH} extrema near 35°N, 40°N, and 45°N-48°N throughout the water column. The southernmost peak is visible along the northern flank of the AC (35°N) where the four uppermost isopycnal surfaces exhibit a dome-like shape (Plate 1). Horizontal diffusion tends to flatten this curvature an lighten the water column. Through vertical stretching, this diffusive effect locally intensifies the equatorward flow V in layer 1, and counteracts it in layers 3 and 4 (Figure 11).

The w_{cH} local minimum (density gain) diagnosed at 40°N across the four uppermost isopycnal surfaces (and at 47°N across 27.4 and 27.6) comes from the local tendency of the isopycnal surfaces to rise northward. Since these minima are not located at exactly the same latitude, their effect on meridional motions is complex and difficult to interpret.

4.3. Adiabatic and Diabatic Motions: Summary

The impact of diffusion on the intergyre circulation is now compared with the adiabatic motion V_{pi} that could exist within the isopycnal layers without any diapycnal mass flux, between solid isopycnal surfaces. Unlike V_{pV} and V_{pH}, which are forced locally by diapycnal eddy fluxes, V_{pi} is forced in the regions where the density layers outcrop (by high latitude convection or Ekman pumping). A motion may thus be considered as adiabatic where V_{pV} and V_{pH} are smaller than V_{pi}.

Figure 11 shows that the meridional stuctures of V and V_{pi} are similar south of about 40°N in layers 1 and 2. Within the SPMW the model behavior is comparable to the idealized ventilated thermocline solutions, but the ventilation of SPMW is slowed by eddy diffusion effects (vertical diffusion in the upper SPMW, horizontal diffusion in the lower SPMW). The situation is comparable north of about 45°N in layer 3, where the realistic poleward flow simulated by the model could exist without diapycnal mixing (V and $V_{pi} > 0$). This corroborates the analytical results of *Schopp and Arhan* [1986] based on the ventilated thermocline adiabatic hypothesis. This flow is probably driven northward by positive Ekman pumping in the subpolar gyre, where our third layer outcrops. As for the SPMW, the model suggests that this motion is slowed down by horizontal diffusion, perhaps too much since V is rather weak. We mentioned above that the observed poleward motion of MW is not simulated by the model between 36°N and 45°N. From a local analysis based on in situ data, *Arhan* [1987] demonstrated that this motion may be driven by salt fingering below the MW intrusion. This mechanism, which generates up gradient density fluxes through differential salinity and temperature vertical diffusion, is not parameterized in the model. If this process is actually at work and significant throughout the basin, the subsequent northward motion is thus not expected to be simulated by the model south of 45°N.

The downward decrease of ρ_z below the main thermocline is likely to induce a downward increase of w_{cV}, a negative V_{pV} through vortex stretching, and a southward motion of diabatic origin within layers 3 and 4. Indeed, within the upper and lower MW, V_{pi} does not follow V as well as within the SPMW.

5. Conclusion

The aims of this work were to describe and validate the mean solution obtained in a coarse-resolution regional model of the eastern North Atlantic, and to investigate the large-scale equilibrium dynamics of the intergyre zone. The computational domain is restricted to the basin of interest through the use of three self-adapting open boundaries that leave the barotropic currents locally unconstrained. The model is integrated over 38 years with a variable surface and baroclinic lateral forcing, and reaches a steady annual-mean state (modulated by the seasonal cycle) despite the wide opening of the basin to the rest of the Atlantic. The final annually averaged circulation, stratification and forcing are adjusted mutually and provide a plausible picture of the ocean mean state in the basin.

The North Atlantic Current (NAC) brings about 40 Sv into the eastern basin above the Mid-Atlantic Ridge (MAR), where it shifts slightly northward. As shown in recent studies, 30% of this transport seem to be induced by topographic effects. East of the MAR the NAC splits into three main branches whose paths and transports agree with different in situ estimates. Two thirds of the NAC recirculates toward the subpolar gyre. A 13-Sv Irminger Current circulates cyclonically and joins the East Greenland Current which transport reaches the realistic value of 40 Sv.

South of about 47°N above 800 m, 4.5 Sv of thermocline waters are advected toward a realistic Azores Current (AC), which transport exceeds 9 Sv across 35°W and decreases eastward. As far as we know, the AC had never been simulated by coarse-resolution models. The combined use of a self-adapting western open boundary that maintains the baroclinic structure of incoming currents and of a *T-S* climatology [*Reynaud et al.*, 1998] that represents the density fronts quite well partly explains this interesting feature. Unlike another wind data set that we used in a sensitivity experiment [*Penduff*, 1998], the wind climatology of *Hellermann and Rosenstein* [1983] also contributes to the presence of the AC since its mean curl forces an eastward flow between

30°N and 35°N (Figure 5). The local entrainment of surface waters into the MW in the Gulf of Cadiz, parameterized by a simple relaxation of tracers, also significantly increases the AC transport. This feature was previously mentioned by *Jia* [2000]. The sensitivity of the AC transport to the wind forcing and to the relaxation in the Gulf of Cadiz confirms that the transport of incoming currents (in particular AC and NAC) is not prescribed along the western self-adapting open boundary but is influenced by interior processes.

South of the NAC above 2000 m the main circulation is correctly simulated. Its dynamical origin was investigated through the buoyancy and vorticity balances. The southward motion of thermocline waters and Subpolar Mode Water agrees with previous studies and is consistent with a ventilated thermocline adiabatic solution, globally slowed down by diffusive effects. A similar dynamical regime is found between 500 and 1000 m north of 45°N, where the flow is directed northward. Positive Ekman pumping in the subpolar gyre is likely to drive this northward motion adiabatically, as shown by *Schopp and Arhan* [1986] with a model of the ventilated thermocline; this flow is slowed down in the present model by eddy diffusive effects. South of 45°N, vertical diffusion induces a slow southward drift of the MW through vortex stretching, instead of the observed northward flow. The absence in the model of any parametrization of salt fingering, a process which could force this motion [*Arhan,* 1987; *Spall,* 1999], is a possible explanation for this discrepancy. Another explanation is the crude representation of the MW overflow process in the Gulf of Cadiz and of the subsequent spreading of the MW into the Atlantic (simple relaxation of tracers and closed boundary near the Strait of Gibraltar, coarse resolution, smoothed topography). The paths and transports of Labrador Sea Water over the basin globally agree with observations.

Our computation of the terms involved in the buoyancy and vorticity balances is rather simple and could be improved. First, our annually averaged solution represents a steady climatological state that is largely modulated by interannual variability in the real ocean, especially within the intergyre zone as noted in the introduction; the use of an multiyear surface forcing would certainly generate a more realistic fluctuating regime in the intergyre zone. On the other hand, the explicit representation of mesoscale eddies, a better vertical resolution, and an efficient parametrization of salt fingering are likely to make the model solution and of our diagnostics more realistic. In the future, an on-line computation of diffusive terms would be necessary to close the buoyancy and vorticity balances, and to quantify the contribution of the mesoscale eddies.

Acknowledgments. Useful discussions with M. Arhan and J. Paillet are gratefully acknowledged. We thank the two anonymous reviewers who contributed to improve the manuscript. This research was supported by a DRET doctoral fellowship for 3 years, and by a SHOM research contract for the fourth year.

References

Arhan, M., On the large scale dynamics of the Mediterranean outflow, *Deep Sea Res.*, *34*, 1187-1208, 1987.

Arhan, M., A. Colin de Verdiere, and H. Mercier, Direct observations of the mean circulation at 48°N in the Atlantic Ocean, *J. Phys. Oceanogr.*, *19*, 161-181, 1989.

Bacon, S., Decadal variability in the outflow from the Nordic Seas to the deep Atlantic Ocean, *Nature*, *394*, 871-874, 1998.

Barnier, B., L. Siefridt, and P. Marchesiello, Thermal forcing for a global ocean circulation model using a three-year climatology of ECMWF analyses, *J. Mar. Syst.*, *6*, 363-380, 1995.

Barnier, B., P. Marchesiello, A.P. de Miranda, J.M. Molines, and M. Coulibaly, A sigma-coordinate primitive equation model for studying the circulation in the South Atlantic, I, Model configuration with error estimates, *Deep Sea Res.*, *45*, 573-608, 1998.

Brügge, B., Near-surface mean ciculation and kinetic energy in the central North Atlantic from drifter data, *J. Geophys. Res.*, *100*, 20,543-20,554, 1995.

Bryan, F.O., C.W. Böning, and W.R. Holland, On the midlatitude circulation in a high-resolution model of the North Atlantic, *J. Phys. Oceanogr.*, *25*, 289-305, 1995.

Dickson, R.R., and J. Brown, The production of North Atlantic Deep Water: Sources, rates, and pathways, *J. Geophys. Res.*, *99*, 12,319-12,341, 1994.

Dickson, R.R., J. Gould, T.J. Müller, and C. Maillard, Estimates of the mean circulation in the deep (> 2000m) layer of the eastern North Atlantic, *Prog. Oceanogr.*, *14*, 103-127, 1985.

DYNAMO Group, DYNAMO, Dynamics of North Atlantic Models: Simulation and assimilation with high resolution models, 334 pp., Inst. für Meereskunde, Kiel, Germany, 1997.

Gana, S., and C. Provost, Circulation and fluxes of the Central Atlantic in 1983/1984 estimated by inverse analysis of "Topogulf" hydrographic data, *J. Mar. Syst.*, *4*, 67-92, 1993.

Gill, A.E., *Atmosphere-Ocean Dynamics*, *Int. Geophys. Ser.*, vol 30, 662 pp., Academic, San Diego, Calif., 1982.

Hellermann, S., and M. Rosenstein, Normal monthly wind stress on the world ocean with error estimates, *J. Phys. Oceanogr.*, *13*, 1093-1104, 1983.

Jia, Y.L., Formation of an Azores Current due to Mediterranean overflow in a modeling study of the North Atlantic, *J. Phys. Oceanogr.*, *30*, 2342-2358, 2000.

Kelly, K., The meandering Gulf Stream as seen by the Geosat altimeter: Surface transport, position and velocity variance from 73°W to 46°W, *J. Geophys. Res.*, *96*, 16,721-16,738, 1991.

Klein, B., and G. Siedler, On the origin of the Azores Current, *J. Geophys. Res.*, *94*, 6159-6168, 1989.

Knochel, H., Développement et validation d'un modèle numérique de circulation océanique à coordonnées σ pour l'étude climatique de l'Atlantique Nord, Ph.D. thesis, 210 pp., Univ. J. Fourier, Grenoble, France, 1998.

Krauss, W., E. Fahrbach, A. Aitsam, J. Elken, and P. Koske, The North Atlantic Current and its associated eddy field southeast of Flemish Cap, *Deep Sea Res.*, *34*, 1163-1185, 1987.

Luyten, J.R., and H. Stommel, Gyres driven by combined wind and buoyancy flux, *J. Phys. Oceanogr.*, *16*, 1551-1560, 1986.

Luyten, J.R., J. Pedlosky, and H. Stommel, The ventilated thermocline, *J. Phys. Oceanogr.*, *13*, 292-309, 1983.

Maillard, C., Atlas hydrologique de l'Atlantique Nord-Est, 32 pp, Inst. Fr. de Rech. pour l'Exploit. de la Mer, Brest, France, 1986.

McCartney, M.S., and L.D. Talley, Warm-to-cold water conversion in the northern North Atlantic Ocean, *J. Phys. Oceanogr.*, *14*, 922-935, 1984.

Orvik, K.A., O. Skagseth, and M. Mork, Atlantic inflow to the Nordic Seas in the Svinoy section, *Int. WOCE Newsl.*, *37*, 18-20, 1999.

Otto, L., and H.M. van Aken, Surface circulation in the northeast Atlantic as observed with drifters, *Deep Sea Res.*, *43*, 467-499, 1996.

Paillet, J., and M. Arhan, Shallow pycnoclines and mode water subduction in the eastern North Atlantic, *J. Phys. Oceanogr.*, *26*, 96-114, 1996.

Paillet, J., and H. Mercier, An inverse model of the eastern North Atlantic general circulation and thermocline ventilation, *Deep Sea Res., Part I*, *44*, 1293-1328, 1997.

Paillet, J., M. Arhan, and M.S. McCartney, Spreading of Labrador Sea Water in the eastern North Atlantic, *J. Geophys. Res.*, *103*, 10,223-10,239, 1998.

Penduff, T., Etude de la dynamique de l'Atlantique Nord-Est à l'aide d'un modèle numérique régional, 261 pp., Ph.D. thesis, Univ. de Bretagne Occidentale, Brest, France, 1998.

Penduff, T., A. Colin de Verdière, and B. Barnier, Self-adapting open boundaries for a sigma coordinate model of the eastern North Atlantic, *J. Geophys. Res.*, *105*, 11,279-11,297, 2000.

Reid, J.L., On the total geostrophic circulation of the North Atlantic Ocean: Flow patterns, tracers and transports, *Prog. Oceanogr.*, *33*, 1-92, 1994.

Reynaud, T., P. Legrand, H. Mercier, and B. Barnier, A new analysis of hydrographic data in the Atlantic and its application to an inverse modelling study, *WOCE Newsl.*, *32*, 29-31, 1998.

Richardson, P.L., and A. Tychensky, Meddy trajectories in the Canary Basin measured during the SEMAPHORE experiment, 1993-1995, *J. Geophys. Res.*, *103*, 25,029-25,045, 1998.

Saunders, P.M., Circulation in the eastern North Atlantic, *J. Mar. Res.*, *40*, suppl., 641-657, 1982.

Saunders, P.M., The flux of Overflow Water through the Charlie-Gibbs Fracture Zone, *J. Geophys. Res.*, *99*, 12,343-12,355, 1994.

Schmitz, W.J., Jr, and M.S. McCartney, On the North Atlantic circulation, *Rev. Geophys.*, *31*(1), 29-49, 1993.

Schopp, R., and M. Arhan, A ventilated middepth circulation model for the eastern North Atlantic, *J. Phys. Oceanogr.*, *16*, 344-357, 1986.

Schott, F.A., and C. Böning, Evaluation of the WOCE model in the western equatorial Atlantic: Upper layer circulation, *J. Geophys. Res.*, *96*, 6993-7004, 1991.

Siedler, G., and R. Onken, Eastern recirculation, in *The Warmwatersphere of the North Atlantic Ocean*, edited by W. Krauss, pp. 339-364, Gebrüder Borntraeger, Stuttgart, Germany, 1996.

Spall, M.A., A simple model of the large-scale circulation of Mediterranean Water and Labrador Sea Water, *Deep Sea Res.*, *46*, 181-204, 1999.

Speer, K.G., J. Gould, and J. LaCasce, Year-long trajectories in the Labrador Sea Water of the eastern North Atlantic Ocean, *Deep Sea Res.*, *46*, 165-179, 1999.

Stommel, H., and A.B. Arons, On the abyssal circulation of the world ocean, II, An idealized model of the circulation pattern and amplitude in oceanic basins, *Deep Sea Res.*, *6*, 217-233, 1960.

Stramma, L., Geostrophic transport in the warm water sphere of the eastern subtropical North Atlantic, *J. Mar. Res.*, *42*, 537-558, 1984.

Sy, A., Investigation of large-scale circulation patterns in the central North Atlantic: The North Atlantic Current, the Azores Current, and the Mediterranean Water plume in the area of the Mid-Atlantic Ridge, *Deep Sea Res.*, *35*, 383-413, 1988.

Sy, A., V. Schauer, and J. Meincke, The North Atlantic Current and its associated hydrographic structure above and eastwards of the Mid-Atlantic Ridge, *Deep Sea Res.*, *39*, 825-853, 1992.

Tréguier, A.M., Kinetic energy analysis of an eddy-resolving, primitive equation model of the North Atlantic, *J. Geophys. Res.*, *97*, 687-701, 1992.

Wegner, G., Geostrophische Oberflächenströmung im nördlichen Nordatlantischen Ozean im internationalen geophysikalischen Jahr 1957/58, *Ber. Dtsch. Wiss. Komm. für Meeresforsch.*, *22*, 411-426, 1973.

Wunsch, C., and D. Roemmich, Is the North Atlantic in Sverdrup Balance? *J. Phys. Oceanogr.*, *15*, 1876-1880, 1985.

B. Barnier, Laboratoire des Écoulements Géophysiques et Industriels, UMR 5519 CNRS, BP 53X, 38041 Grenoble Cedex, France. (Bernard.Barnier@hmg.inpg.fr)

A. Colin de Verdière, Laboratoire de Physique des Océans, UMR 6523, Université-CNRS-IFREMER, Université de Bretagne Occidentale, 29285 Brest, France. (Alain.Colin-De-Verdiere@univ-brest.fr)

T. Penduff, Center for Ocean-Atmospheric Prediction Studies, Florida State University, R.M. Johnson Building, 2035 E. Paul Dirac, Suite 200, Tallahassee, FL 32306-2840, USA. (tpenduff@coaps.fsu.edu)

(Received March 30, 2000; revised June 7, 2001; accepted June 14, 2001.)